A metabolomic and proteomic study to elucidate the molecular mechanisms of immunotherapy resistance in patients with oesophageal squamous cell carcinoma

LIJUAN GAO and YONGSHUN CHEN

Department of Clinical Oncology, Renmin Hospital of Wuhan University, Wuhan University First Clinical College, Wuhan, Hubei 430060, P.R. China

Received November 8, 2022; Accepted February 24, 2023

DOI: 10.3892/br.2023.1619

Abstract. Systemic chemotherapy, the standard first-line treatment option for patients with advanced oesophageal squamous cell carcinoma (OSCC), results in a median survival of ~1 year. Immune checkpoint inhibitors are a breakthrough oncology treatment option; however, most patients with advanced OSCC develop primary and acquired resistance to programmed death receptor-1 (PD-1) monoclonal antibody, severely affecting their prognosis. Therefore, there is an urgent need to investigate the molecular mechanism underlying resistance to treatment. The present study aimed to explore the mechanism of resistance to PD-1 monoclonal antibody. Plasma samples were collected from patients with OSCC treated with immunotherapy, who achieved pathological response/partial response (CR/PR) or stable disease/progressive disease (SD/PD) after the fourth treatment cycle. TM-widely targeted metabolomics, widely targeted lipidomics, and DIA proteomics assays were performed. Differential metabolites were screened based on fold change (FC) ≥1.5 or ≤0.67 and a VIP ≥1; differential proteins were screened based on FC >1.5 or <0.67 and P<0.05. The identified metabolites were annotated and mapped using the Kyoto Encyclopedia of Genes and Genomes (KEGG) pathway databases. The differential proteins were annotated to the Gene Ontology and KEGG pathway databases. A correlation network diagram was drawn using differential expressed proteins and metabolites with (Pearson correlation coefficient) r>0.80 and P<0.05. Finally, 197 and 113 differential metabolites and proteins were screened, respectively, in patients with CR/PR and SD/PD groups. The KEGG enrichment analysis revealed that all of these metabolites and proteins were enriched in cholesterol metabolism and in the NF-κB and phospholipase D signalling pathways. The present study is the first to demonstrate that PD-1 inhibitor resistance may be attributed to cholesterol metabolism or NF-κB and phospholipase D signalling pathway activation. This finding suggests that targeting these signalling pathways may be a promising novel therapeutic approach in OSCC which may improve prognosis in patients undergoing immunotherapy.

Correspondence to: Professor Yongshun Chen, Department of Clinical Oncology, Renmin Hospital of Wuhan University, Wuhan University First Clinical College, 238 Jiefang Road, Wuhan, Hubei 430060, P.R. China
E-mail: 2018203020082@whu.edu.cn

Key words: oesophageal squamous cell carcinoma, immunotherapy, PD-1 monoclonal antibody, proteomics, metabolics

Introduction

Systemic chemotherapy, the first-line standard treatment for advanced oesophageal cancer, leads to a median survival of only ~1 year. Immune checkpoint inhibitors (ICIs) have emerged as a breakthrough therapy for tumours resulting in impressive progress in the treatment of multiple tumour types (1-3). Commonly used ICIs include anti-cytotoxic T lymphocyte antigen-4 (CTLA-4), anti-programmed death receptor-1 (PD-1), and anti-programmed death receptor ligand-1 (PD-L1) antibodies. Anti-PD-1 monoclonal antibodies significantly improve therapeutic efficacy in advanced oesophageal cancer, and three phase III clinical trials, KEYNOTE-181 (4), ATTRACTION-3 (5), and ESCORT (6), have confirmed that second-line treatment with anti-PD-1 monoclonal antibodies significantly improved the survival benefit in some patients with advanced oesophageal cancer, confirming the important role of anti-PD-1 monoclonal antibodies in the treatment of advanced oesophageal cancer. The recent KEYNOTE-590 (7) and ESCORT-1st (8) studies also found that anti-PD-1 monoclonal antibodies in combination with chemotherapy as first-line treatment of advanced oesophageal cancer significantly prolonged overall survival (OS) and led to a median OS of 13-16 months. However, the tumour overall response rate (ORR) and median progression-free survival (mPFS) in patients with advanced oesophageal cancer undergoing second-line treatment with anti-PD-1 monoclonal antibodies were ~20% and ~2 months, respectively. The corresponding data for patients with advanced oesophageal cancer undergoing first-line treatment with anti-PD-1 monoclonal antibodies combined with chemotherapy were ~50% and ~6 months, respectively (7,8). These findings indicate that most patients with advanced oesophageal cancer develop

primary and acquired resistance against anti-PD-1 monoclonal antibodies. Therefore, it is important to examine the molecular mechanisms of anti-PD-1 monoclonal antibody resistance in oesophageal cancer to improve patient prognosis.

Metabolomics is an emerging histological discipline that, together with genomics and proteomics, forms the cornerstone of systems biology. It analyses the metabolic status of the whole or the system by means of high-throughput detection and assessment of the dynamics of thousands of low-molecular-weight metabolites that are formed via chemical transformation under certain metabolic conditions (9,10). More precisely, metabolomics is used to identify and quantify metabolites for revealing the association between metabolite changes and pathological states, or for revealing the effects of external factors. Metabolomics holds great application potential as an advanced analytical technique and bioinformatics tool for the diagnosis of various cancers, such as non-small cell lung cancer (11), colorectal cancer (12) and gastric cancer (13). Analytical techniques in metabolomics mainly include nuclear magnetic resonance (NMR), gas chromatography-mass spectrometry (GC-MS), and liquid chromatography-mass spectrometry (LC-MS), which have different characteristics and technical limitations. In particular, MS techniques, such as GC-MS and LC-MS, have the advantages of high sensitivity and a wide detection range with a simple and useful database for metabolite identification (14-18). NMR spectroscopy allows rapid and high-throughput detection with relatively high reproducibility while requiring a small number of samples and being non-destructive to the samples, and is therefore suitable for tissue analysis (19).

Data-independent acquisition mass spectrometry (DIA-MS) is a next-generation proteomic method that generates permanent digital proteomic maps, allowing highly reproducible retrospective analysis of cell and tissue samples (20). The technology has been widely used in oncology research to elucidate the mechanisms of cancer development (21), mechanisms of drug resistance, molecular classification of cancer, and screening of cancer biomarkers (22). The number of applications of DIA-MS to cancer proteomics has continually increased since the introduction of this technology in 2012 and includes different cancer types such as colorectal cancer (23,24), hepatocellular carcinoma (25), pancreatic cancer (26), prostate cancer (27), and follicular thyroid tumours (28).

In the present study, plasma samples were collected from 15/16 patients with a pathological report confirming complete response/partial response (CR/PR) or stable disease/progressive disease (SD/PD) after immunotherapy. Metabolomic and proteomic assays were performed on the plasma samples to elucidate the changes in protein expression and metabolite expression within the CR/PR group vs. the PD/SD group. This is the first time a multi-omics technique has been used to explore proteins and metabolites associated with resistance to PD-1 monoclonal antibody in patients with oesophageal squamous cell carcinoma (OSCC).

Materials and methods

Study design. In order to explore the molecular mechanism of immunotherapy resistance in OSCC, plasma samples were collected from patients with OSCC who underwent treatment with an anti-PD-1 monoclonal antibody combined with chemotherapy after the fourth treatment cycle between January 2021 and January 2022. The cohort was comprised of 31 patients including 8 females and 23 males. Their ages ranged from 42 to 80 with a median age of 65 years. The inclusion criteria were as follows: i) Age, 18 to 80 years; ii) Eastern Cooperative Oncology Group (ECOG) performance status (PS) score 0 to 1 (29); iii) history or pathology confirmed ESCC; iv) chemotherapy regimen consisted of cisplatin plus 5-fluorouracil; and v) no previous tumor-related treatments. The exclusion criteria were: i) esophageal adenocarcinoma and small-cell carcinoma; and ii) incomplete follow-up data. The treatment efficacy was evaluated by the Responsive Evaluation Criteria in Solid Tumours (RECIST) 1.1 (30) at the same period. Finally, the plasma samples were divided into the CR/PR group (n=15) and the SD/PD group (n=16). Subsequently, the differentially expressed proteins (DEPs) and differentially expressed metabolites (DEMs) between the two groups, which may be the main contributing factors to immunotherapy resistance, were determined using proteomic (DIA proteomics) and metabolic analysis (including TM-widely targeted metabolomics and widely targeted lipidomics). Furthermore, the DEPs and DEMs were annotated to Kyoto Encyclopedia of Genes and Genomes (KEGG) enrichment analysis and the molecular mechanisms were elucidated by conjoint analysis of the DEPs and DEMs. The study work flow is illustrated in Fig. 1.

Sample collection. A total of 31 plasma samples of oesophageal squamous cell carcinoma, including 15 CR/PR and 16 SD/PD who underwent PD-1 monoclonal antibody combined with chemotherapy were collected. The CR, PR, SD, PD was determined using RECIST 1.1. TNM staging was performed according to the sixth Union for International Cancer Control (UICC) TNM classification system (31) due to the large span of diagnosis. All oesophageal samples were collected from patients at Renmin Hospital of Wuhan University (Wuhan, China) between January 2021 and January 2022. Blood was collected after obtaining written informed consent from the participants. All patient consents were provided by the participants themselves or their guardian. The present study was performed in accordance with the Declaration of Helsinki, and the study was approved (approval no. WDRY2020-K212) by the Bioethics Committee of Renmin Hospital of Wuhan University (Wuhan, China). Detailed clinicopathological data and qualified blood samples were available for all participants. The sample details are provided in Table I. All samples were immediately stored at -80˚C until further analysis. The workflow of the present study is presented in Fig. 1.

TM-widely targeted metabolomics

Sample extraction. The steps for sample extraction were as follows: i) The sample was removed from the -80˚C refrigerator and placed on ice until no pieces of ice were observed in the sample (all subsequent operations were required to be performed on ice). ii) After thawing, the sample was shaken on a vortex mixer for 10 sec to ensure thorough mixing, and then 50 μl of the sample was transferred to a centrifuge tube numbered correspondingly. iii) A metabolite extraction agent (300 μl, 20/80 acetonitrile/methanol solution) containing internal standards was added to the centrifuge tube, shaken

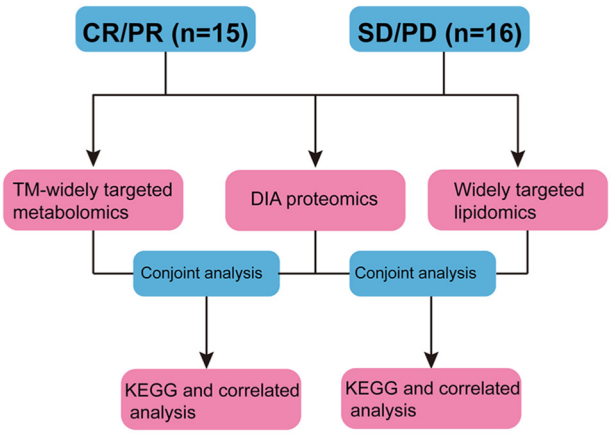

Figure 1. Workflow of the present study. The plasmas of patients with oesophageal squamous cell carcinoma, who were treatment with anti-programmed death receptor-1 monoclonal antibody combined with chemotherapy after the fourth treatment cycle, were collected. The curative effect was simultaneously determined by the Responsive Evaluation Criteria in Solid Tumours 1.1 at the same period. Finally, the plasma samples were divided into a complete response/partial response group (n=15) and a stable disease/progressive disease group (n=16). The DEPs and DEMs between the two groups, which may mainly contribute to the immunotherapy resistance, were then identified by proteomic (data-independent acquisition proteomics) and metabolic (including TM-widely targeted metabolomics and widely targeted lipidomics) analysis. Furthermore, conjoint analysis of the DEPs and DEMs included Kyoto Encyclopedia of Genes and Genomes enrichment pathway analysis and correlated analysis was used to elucidate the molecular mechanisms. CR/PR, complete response/partial response; SD/PD, stable disease/progressive disease; DEPs, differentially expressed proteins; DEMs, differentially expressed metabolites; DIA, data-independent acquisition; KEGG, Kyoto Encyclopedia of Genes and Genomes.

on the vortex mixer for 3 min, and centrifuged at 1,609.92 x g for 10 min at 4˚C. iv) Following centrifugation, 200 μl of the supernatant was transferred into another correspondingly numbered tube, which was then allowed to stand for 30 min at -20˚C in the refrigerator. v) The aforementioned tube was centrifuged at 1,609.92 x g for 3 min at 4˚C, then 180 μl of supernatant was transferred into the liner tube of the corresponding injection vial for instrumental analysis.

LC-MS operating conditions for metabolite detection. The samples were firstly analysed by a non-targeted metabolite to enlarge the database for widely targeted metabolites. Non-targeted metabolite detection was conducted using ultra performance liquid chromatography (UPLC; ExionLC AD; https://sciex.com.cn/) coupled with quadrupole-time of flight mass spectrometry (TripleTOF 6600; AB SCIEX). The operating conditions of UPLC were as follows: ACQUITY HSS T3 columns (2.1x100 mm, 1.8 μm), 0.1% formic acid/water as mobile phase A, 0.1% formic acid/acetonitrile as mobile phase B, column temperature of 40˚C, flow rate of 0.35 ml/min, and injection volume of 5 μl.

The data acquisition instrumentation system for widely targeted metabolomics primarily comprised a UPLC instrument (ExionLC AD; https://sciex.com.cn/) coupled with a tandem mass spectrometry (MS/MS) instrument (QTRAP®; https://sciex.com/).

Chromatographic separation conditions were as follows: i) a Waters ACQUITY UPLC HSS T3 C18 column (1.8 μm; 2.1x100 mm) as the chromatography column; ii) ultra-pure water (containing 0.1% formic acid) as phase A and acetonitrile (containing 0.1% formic acid) as phase B; iii) a mobile-phase gradient with water/acetonitrile (V/V) of 95:5 at 0 min, 10:90 at 11.0 min, 10:90 at 12.0 min, 95:5 at 12.1 min, and 95:5 at 14.0 min; and iv) mobile-phase flow rate of 0.35 ml/min, column temperature of 40˚C, and injection volume of 2 μl.

MS conditions. The electrospray ionization (ESI) source temperature was 500˚C, with an ion spray voltage of 5,500 V for the positive mode and -4,500 V for the negative mode. The ion source gas I (GS I) and gas II (GS II) pressures were both 50 psi, and the curtain gas (CUR) pressure was 25 psi. Collision-activated dissociation (CAD) parameters were set to high values. In the triple quadrupole (Qtrap), each ion pair was scanned for detection based on the optimized declustering potential (DP) and collision energy (CE).

Widely targeted lipidomics

Sample extraction. The steps for sample extraction were as follows: i) The sample was removed from the -80˚C refrigerator and placed on ice until no pieces of ice were observed in the sample. ii) After thawing, the sample was shaken on a vortex mixer for 10 sec to ensure thorough mixing, and then 50 μl of the sample was transferred to a centrifuge tube numbered accordingly. iii) To the centrifuge tube 1 ml of lipid extraction buffer (methyl tert-butyl ether/methanol=3:1, V/V) was added containing internal standards, followed by shaking the resulting mixture on a vortex mixer for 15 min. iv) To the above mixture 200 μl of water was added, and the new mixture was shaken on a vortex mixer for 1 min, followed by centrifugation at 1,609.92 x g for 10 min at 4˚C. v) Following centrifugation, 200 μl of the supernatant was transferred into a correspondingly numbered centrifuge tube and concentrated until completely dry. vi) To the aforementioned centrifuge tube, 200 μl of mobile phase B was added, and the mixture was shaken on a vortex mixer for 3 min, followed by centrifugation at 1,609.92 x g for 10 min at 4˚C, and then by sampling of the supernatant for LC-MS/MS analysis.

Data acquisition conditions of metabolites. The data acquisition instrumentation system consisted primarily of a UPLC instrument (ExionLC AD) coupled with a tandem mass spectrometry (MS/MS) instrument (QTRAP®).

Liquid phase conditions were mainly the following: i) A Thermo Accucore™ C30 column (2.6 μm, 2.1x100 mm) as the chromatography column; ii) acetonitrile/water (60/40, V/V; containing 0.1% formic acid and 10 mmol/l ammonium formate) as mobile phase A, and acetonitrile/isopropanol (10/90, V/V) (containing 0.1% formic acid and 10 mmol/l ammonium formate) as mobile phase B; iii) a mobile-phase gradient with A/B (V/V) of 80:20 at 0 min, 70:30 at 2 min, 40:60 at 4 min, 15:85 at 9 min, 10:90 at 14 min, 5:95 at 15.5 min, 5:95 at 17.3 min, 80:20 at 17.5 min, and 80:20 at 20 min; iv) a mobile-phase flow rate of 0.35 ml/min, column temperature of 45˚C, and injection volume of 2 μl.

MS conditions were mainly the following: The ESI source temperature was 500˚C, with an ion spray voltage of 5,500 V for the positive mode and -4,500 V for the negative mode.

Table I. Clinicopathological characteristics of patients with oesophageal squamous cell carcinoma.

	CR/PR (n=15)	SD/PD (n=16)
Age (%)		
<65	10 (66.7)	8 (50.0)
≥65	5 (33.3)	8 (50.0)
Sex (%)		
Female	2 (13.3)	6 (37.5)
Male	13 (86.7)	10 (62.5)
TNM stage (%)		
Stage I	1 (6.7)	0 (0.0)
Stage II	2 (13.3)	2 (12.5)
Stage III	4 (26.7)	8 (50.0)
Stage IV	8 (53.3)	6 (37.5)

CR/PR, complete response/partial response; SD/PD, stable disease/progressive disease.

The ion source GS I and GS II pressures were 45 psi and 55 psi, respectively, and the CUR pressure was 25 psi. CAD parameters were set to medium values. In the Qtrap, each ion pair was scanned for detection based on the optimized DP and CE.

Metabolite identification and quantification and data analysis. After MS data were analysed with software Analyst 1.6.3 (AB SCIEX), substances were accurately identified by mass-to-charge ratio (m/z) and RT of multiple ion pairs and second spectra of the identified metabolites using the self-built target standard database MWDB (including secondary spectra and RT), the public MHK database compiled by Metware [comprising Metlin, Human Metabolome Database (HMDB), and KEGG databases and including secondary spectra and RT], and the MetDNA algorithm.

After screening the characteristic ions of each substance by triple quadrupole, the signal strength of characteristic ions in the detector was obtained. Subsequently, through integrating and correcting chromatographic peaks using the software MultiQuant (version 3.0.3; AB SCIEX), the relative content of the corresponding substance represented by the area of each chromatographic peak, was obtained.

Significantly regulated metabolites between groups were determined by variable importance in projection (VIP) ≥1 and absolute Log2FC ≥1.5 or ≤0.67. VIP values were extracted from Orthogonal Partial Least Squares Discriminant Analysis (OPLS-DA) results, which also contain score plots and permutation plots, and permutation plots were generated using R package MetaboAnalystR (version 1.0.1; https://www.metaboanalyst.ca/). The data was log transformed (log2) and mean centering was performed before OPLS-DA. In order to avoid overfitting, a permutation test (200 permutations) was performed. Metabolite annotation was performed based on the KEGG compound database (http://www.kegg.jp/kegg/compound/).

Quantitative proteomics

Sample extraction. Lysis solution (8 M urea/100 mM Tris-Cl) was added to the sample. The resulting mixture was sonicated in a water bath and incubated with dithiothreitol (DTT) for 1 h at 37˚C. Next, iodoacetamide (IAA) was added and the alkylation reaction was allowed to take place at room temperature in the dark to block the sulfhydryl groups. Protein concentration was determined using the Bradford method. After protein quantification, 50 μg of the protein sample was used for sodium dodecyl-sulphate polyacrylamide gel electrophoresis (5% concentrated gel; 12% separation gel), which was based on observation of Coomassie brilliant, blue-stained protein bands. After sample reduction and alkylation, 100 mM Tris-HCl was added to the sample to dilute the urea concentration to <2 M. Trypsin was added at an enzyme-to-protein mass ratio of 1:50 and the mixture was incubated overnight at 37˚C for enzymatic protein cleavage, which was terminated the next day by adding 10% TFA. The supernatant was desalted with Sep-Pak C18, suction-dried, and stored at -20˚C for later use.

MS detection. MS data were acquired using an Orbitrap Exploris 480 mass spectrometer in tandem with an EASY-nLC 1200 LC system (Thermo Fisher Scientific, Inc.). Peptide samples were solubilized by a loading buffer, aspirated by an autosampler, and loaded to an analytical column (75 μm x25 cm, C18, 1.9 μm, 100 Å) for separation. Two mobile phases (mobile phase A, 0.1% formic acid; mobile phase B, 0.1% formic acid with 80% acetonitrile) were used in a gradient. The flow rate of each liquid phase was set to 300 nl/min. MS data were acquired in DIA mode, with each scan cycle consisting of one MS1 scan (R=60K, AGC=3e6, Max IT=30 msec, scan range=350-1,250 m/z) and 40 MS2 scans of variable windows (R=30K, AGC=1,000%, Max IT=50 msec). High field asymmetric waveform ion mobility spectrometry (FAIMS) was operated (CV-45) and the collision energy was set to 30.

Data analysis. Raw DIA data were analysed using software DIA-NN (v1.8) (32) according to the following steps: i) A spectral library was predicted from the Swiss-Prot human database (which was reviewed on March 12, 2021) by using the DL algorithm of DIA-NN; ii) protein and peptide ions were identified from the predicted library using the match between run (MBR) algorithm with the raw DIA data; iii) the protein and peptide ion identifications were filtered at a 1% false discovery rate (FDR) to obtain quantitative proteomic information for subsequent analysis.

A sample reproducibility test was performed using PCA analysis and correlation coefficient analysis (Pearson correlation test) based on the relative quantification results of protein. The mean expression level of a given protein across all biological replicates in one group was divided by the counterpart in the other group, and the ratio was defined as the fold change (FC), with FC <0.67 or FC >1.5 as the threshold for differential expression of proteins in the two groups. A T-test on the FC data, with $P<0.05$ considered indicative of statistical significance, was performed to identify differentially expressed proteins DEPs. Functional enrichment analysis of DEPs was performed to identify the Gene Ontology (GO; http://www.geneontology.org/) categories and KEGG pathways (clusterProfiler 3.10.1; https://bioconductor.org/packages/release/bioc/html/clusterProfiler.html).

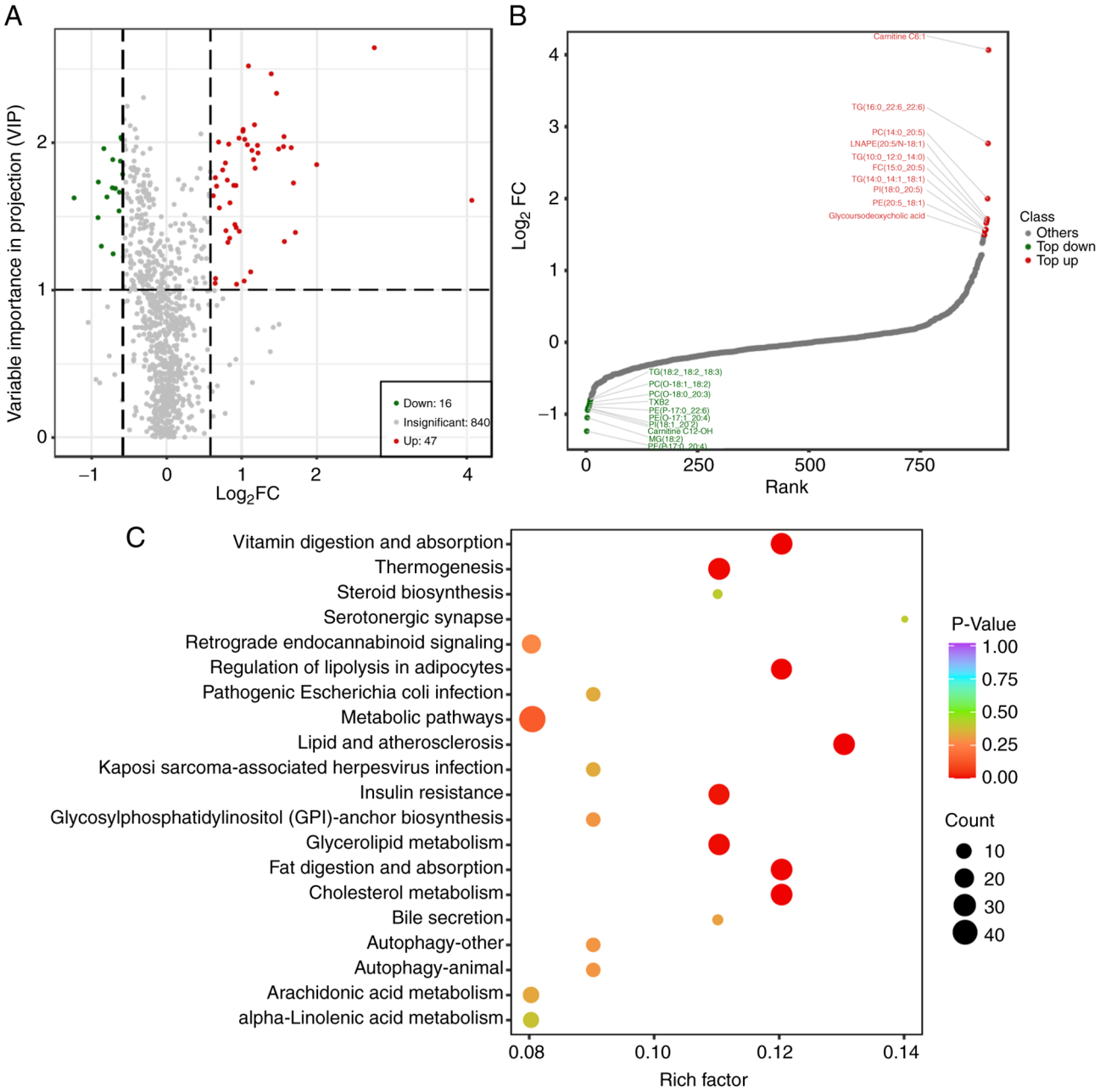

Figure 2. Metabolic change analysis of stable disease/progressive disease vs. complete response/partial response using TM-widely targeted metabolomics. (A) The volcano plot shows the DEMs in the two groups. Each dot in the volcano map represents a metabolite, with the green dots representing downregulated differential metabolites, the red dots representing upregulated differential metabolites, and the grey dots representing detected but not significantly different metabolites. The x-coordinate represents the logarithmic value (log2FC) of the multiple of the relative content difference of a certain metabolite in the two groups of samples. The greater the absolute value of the x-coordinate is, the greater the relative content difference of the substance between the two groups of samples. Under VIP + FC (fold change) double screening conditions: The ordinate represents the VIP value, and the larger the ordinate value, the more significant the difference, and the more reliable the differentially expressed metabolites obtained by screening. (B) The top 10 up- and downregulated DEMs of the two groups. The horizontal coordinate represents the cumulative number of substances ordered according to the difference multiple from the smallest to the largest, and the vertical coordinate represents the pair value with the difference multiple as base 2. Each point represents a substance; the green points represent the top 10 downregulated substances, and the red points represent the top 10 upregulated substances. (C) The Kyoto Encyclopedia of Genes and Genomes pathway enrichment analysis of the DEMs. The rich factor is the ratio of the number of DEMs in the corresponding pathway to the total number of metabolites detected by the pathway. The higher the value, the greater the enrichment degree. The abscissa represents the rich factor corresponding to each pathway; the ordinate represents the pathway name; the colour of the dots is the P-value; the redder it is, the more significant the enrichment is. The size of the dot represents the number of enriched differential metabolites. DEMs, differentially expressed metabolites; VIP, variable importance in projection.

Results

Metabolomic changes in the SD/PD group relative to the CR/PR group. Widely targeted metabolomics and lipidomics were performed on the plasma samples of the CR/PR and PD/SD groups of patients with OSCC to elucidate the metabolomic differences between the two groups. A total of 904 metabolites belonging to the lipid family, including sterol lipid, fatty acyl class, glycerol phospholipids, sphingolipid, and glyceride class were identified by wildly targeted lipids.

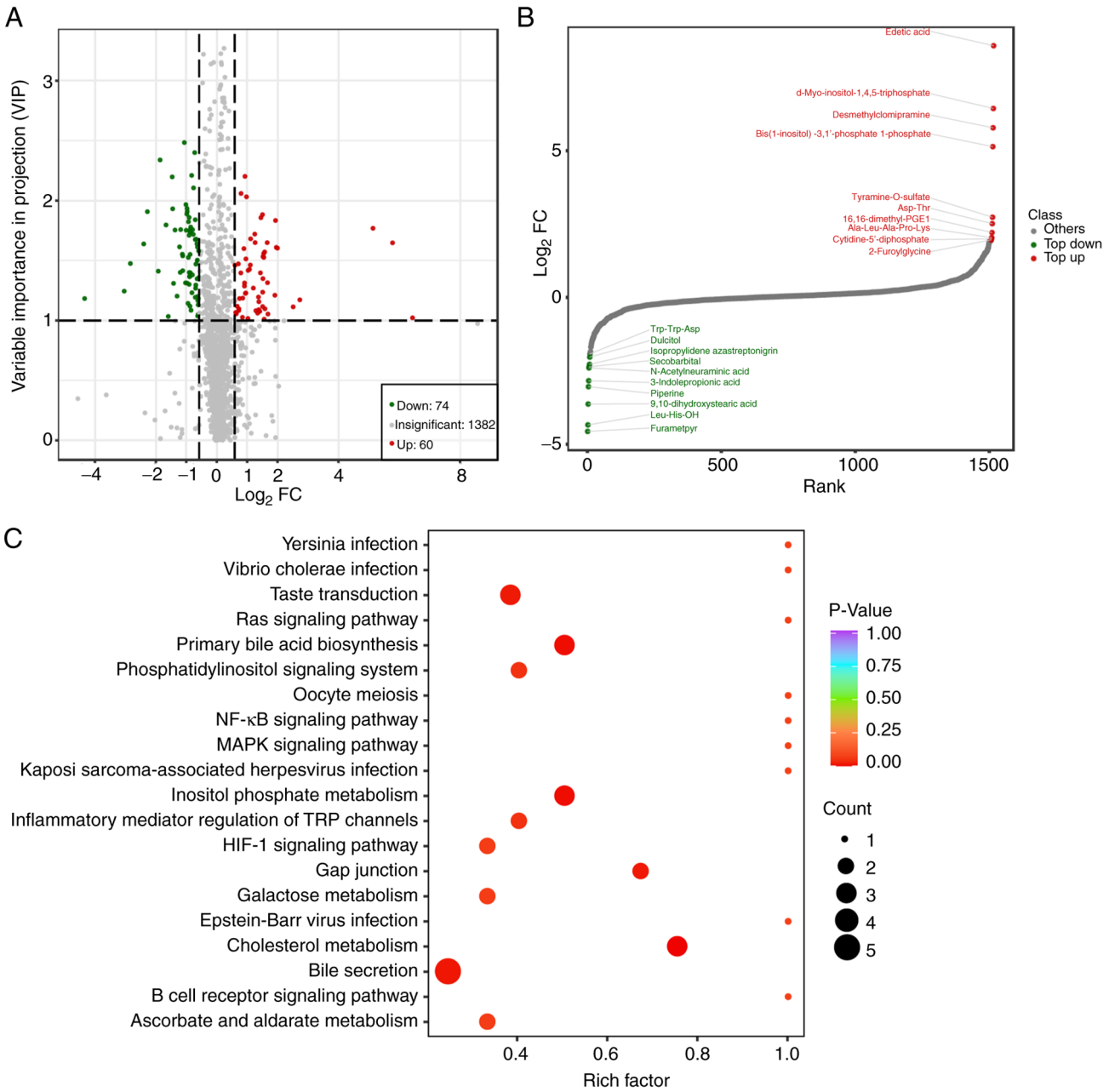

Figure 3. Metabolic change analysis of stable disease/progressive disease vs. complete response/partial response using widely targeted lipidomics. (A) The Volcano plot shows the DEMs in the two groups. Each dot in the volcano map represents a metabolite, with the green dots representing downregulated differential metabolites, the red dots representing upregulated differential metabolites, and the grey dots representing detected but not significantly different metabolites. The x-coordinate represents the logarithmic value (log2FC) of the multiple of the relative content difference of a certain metabolite in the two groups of samples. The greater the absolute value of the x-coordinate is, the greater the relative content difference of the substance between the two groups of samples. Under VIP + FC (fold change) double screening conditions: The ordinate represents the VIP value, and the larger the ordinate value, the more significant the difference, and the more reliable the DEMs obtained by screening. (B) The top10 up- and downregulated DEMs of the two groups. The horizontal coordinate represents the cumulative number of substances ordered according to the difference multiple from the smallest to the largest, and the vertical coordinate represents the pair value with the difference multiple as base 2. Each point represents a substance; the green points represent the top 10 downregulated substances, and the red points represent the top 10 upregulated substances. (C) The Kyoto Encyclopedia of Genes and Genomes pathway enrichment analysis of the DEMs. The rich factor is the ratio of the number of DEMs in the corresponding pathway to the total number of metabolites detected by the pathway. The higher the value, the greater the enrichment degree. The abscissa represents the rich factor corresponding to each pathway; the ordinate represents the pathway name; the colour of the dots is the P-value; the redder it is, the more significant the enrichment is. The size of the dot represents the number of enriched differential metabolites. DEMs, differentially expressed metabolites; VIP, variable importance in projection.

A total of 1,517 metabolites were detected by TM-widely targeted metabolomics, including bile acids, amino acid, phenolic acids, nucleotide, and its metabolites.

As shown in the volcano plot, a total of 16 downregulated metabolites and 47 upregulated metabolites were detected by widely targeted lipidomics (Fig. 2A). The upregulated differentially expressed metabolites were mainly Carnitine C6:1, TG(16:0 22:6), PC(14:0-20:5), LNAPE(20:5/N-18:1), TG(10:0-12:0_14;0), PC(15:0_20:5), TG(14:0,_14:1_18:1), PI(18: 0,_20:5), PE(20:5_18:1), and PE(16:0_20:5), and the downregulated differentially expressed metabolites were mainly LPI(20:3/0:0), PE(18:2,_19:1), PC(15:0_20:3),

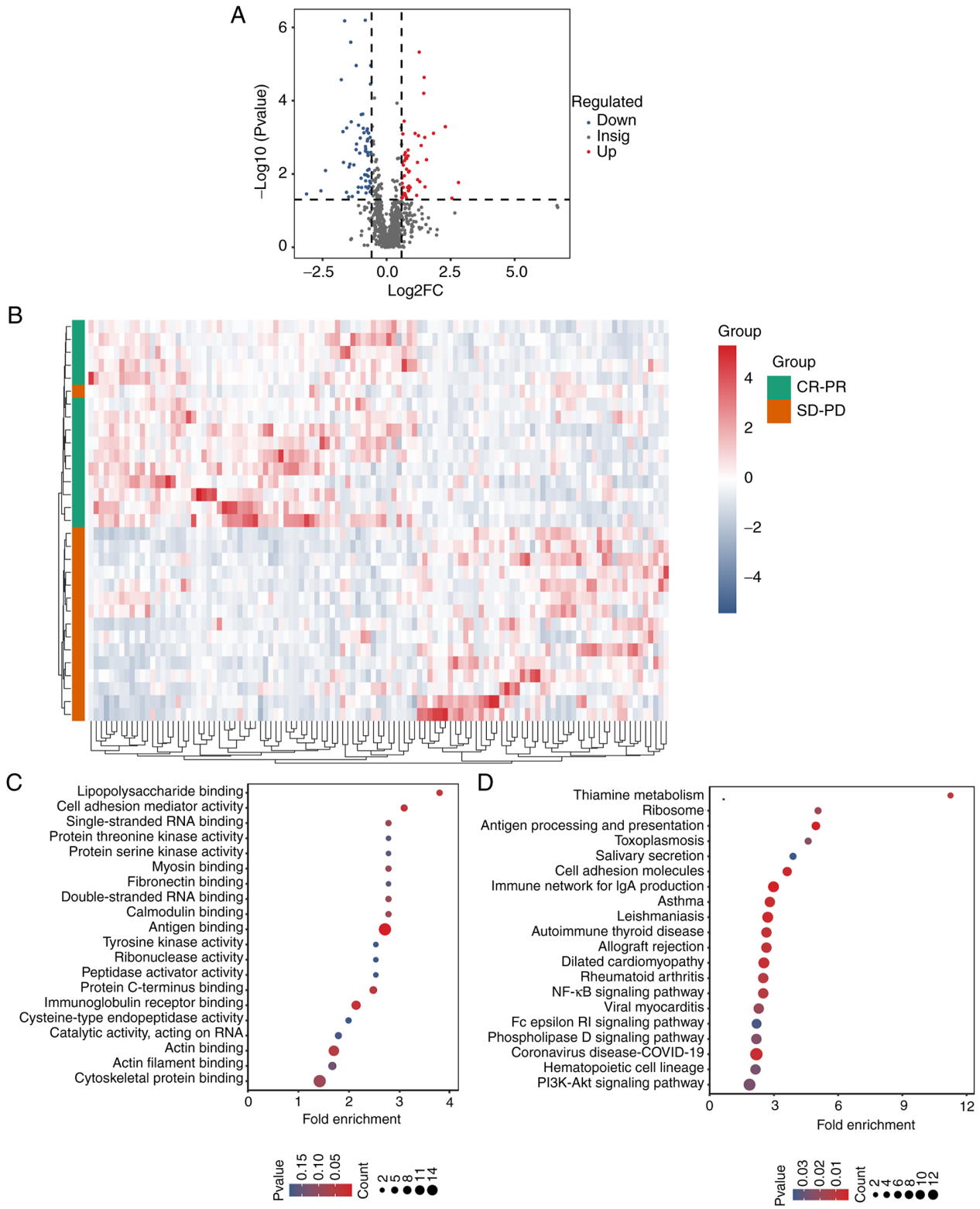

Figure 4. Protein profiling changes of stable disease/progressive disease vs. complete response/partial response using quantitative proteomics. (A) The volcano plot shows the DEPs in the two groups. The horizontal coordinate represents log2FC, the vertical coordinate represents-log10(P-value), the red and blue scatter plots represent the upregulated and downregulated proteins, respectively, and the dark grey scatter plots represent the non-significantly expressed proteins. (B) The heat map of the protein profiling of the two groups. The row represents the protein cluster, the column represents the sample cluster, and the shorter the cluster branch, the larger the similarity. (C) The top 20 GO biological processes of the DEPs. The x-coordinate represents the enrichment ratio (GeneRatio/BgRatio). The greater the enrichment ratio, the greater the degree of enrichment of the differential protein. The y-coordinate represents the enriched GO items. The change of dot colour from blue to red represents the change in the P-value from large to small. The smaller the P-value, the more statistically significant it is. The size of the dot represents the number of different proteins annotated by the corresponding item. (D) The top 20 KEGG pathways of the DEPs. The x-coordinate represents the enrichment ratio (GeneRatio/BgRatio). The larger the enrichment ratio is, the higher the enrichment degree of differential protein is. The y-coordinate represents the enriched KEGG pathway. The change of dot colour from blue to red represents the change of the P-value from large to small. The smaller the P-value is, the more statistically significant it is. The size of the dot represents the number of different proteins in the corresponding functional annotation. DEPs, differentially expressed proteins; GO, Gene Ontology; KEGG, Kyoto Encyclopedia of Genes and Genomes; SD-PD, stable disease-progressive disease; CR-PR, complete response-partial response.

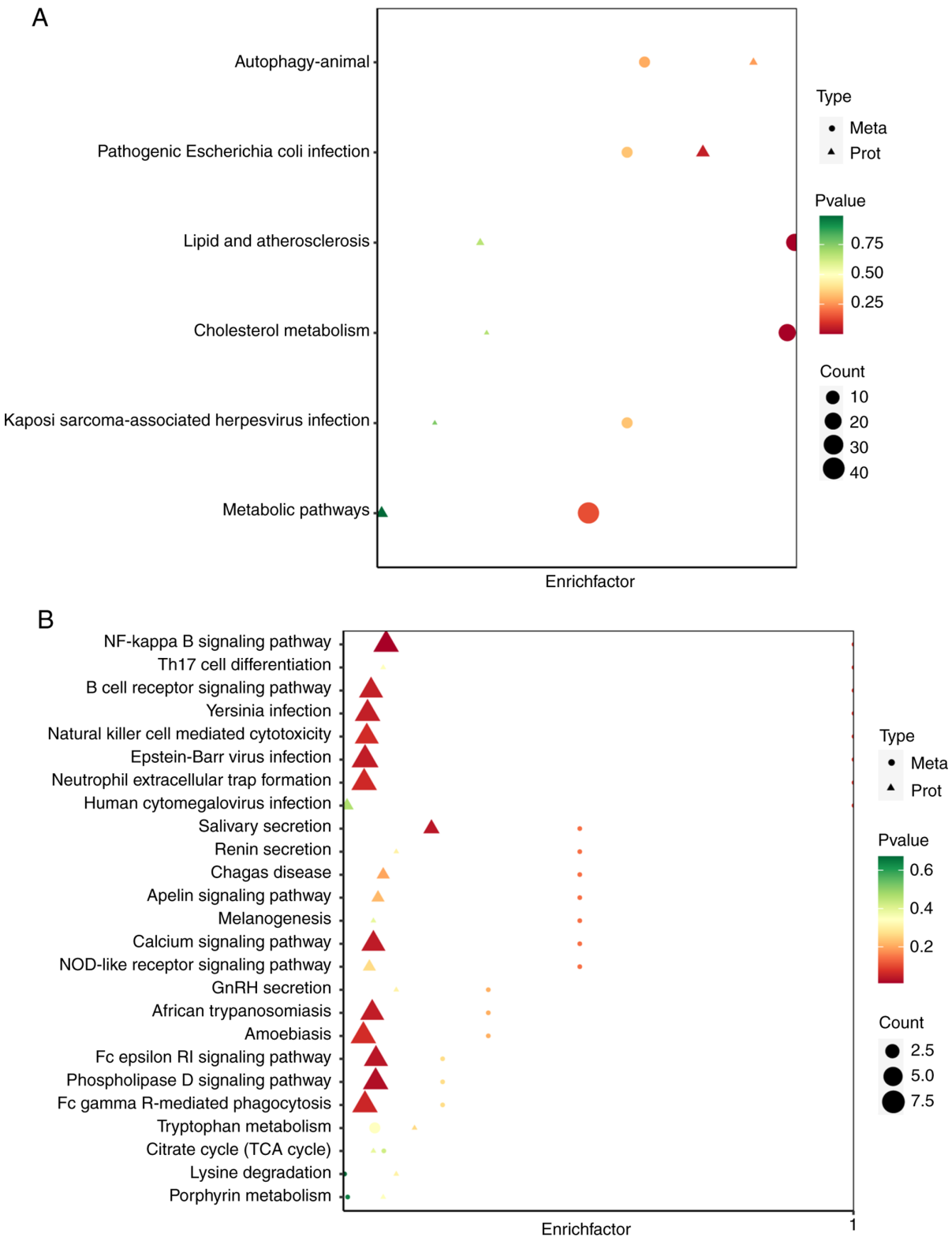

Figure 5. Conjoint analyses of the metabolics and proteomics data. (A and B) The bubble diagram shows the co-enrichment KEGG pathways of the diferentially expressed metabolites and the differentially expressed proteins of the (A) widely targeted lipidomics and (B) TM-widely targeted metabolomics. The x-coordinate represents the enrichment factors (Diff/Background) of the pathway in different omics, and the y-coordinate represents the names of KEGG pathways. The gradient of red, yellow and green represents the change of enrichment significance from high to medium to low, which is represented by the P-value. The shape of the bubble represents different omics, and the size of the bubble represents the number of different metabolites or proteins, and the larger the number, the larger the dot. KEGG, Kyoto Encyclopedia of Genes and Genomes.

Carnitine C10:1-OH, PC(O-18:1_18;2), PC(O-18:0-20:3), TXB2, PE(O-17:1_20:4), PI(18:1_20:2), and PE(P-17:0_20:4; (Fig. 2B). KEGG enrichment analysis of the differentially expressed metabolites showed that these were mainly enriched in the primary bile acid biosynthesis pathway and the bile secretion pathway, as well as the cholesterol metabolism

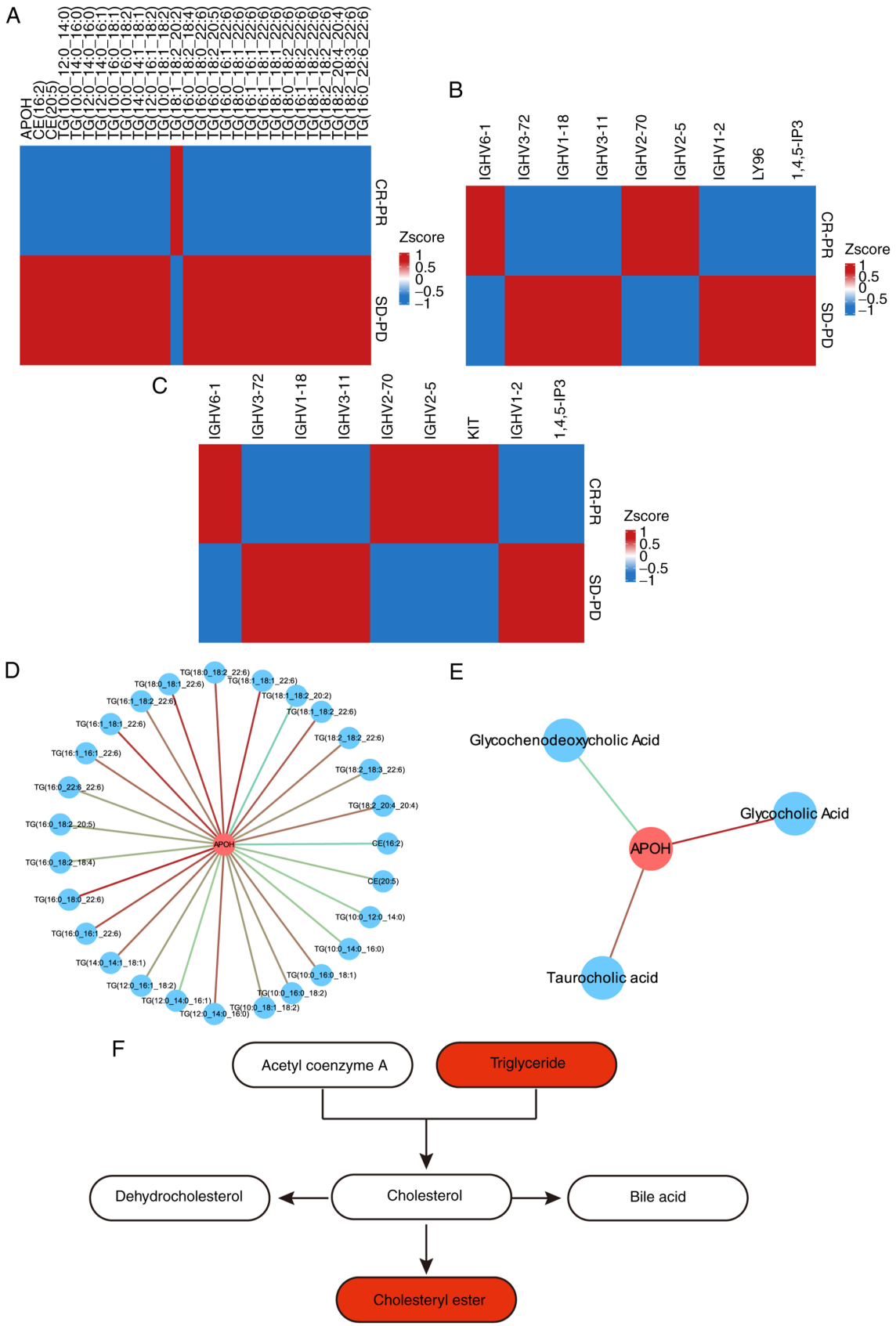

Figure 6. Enrichment of DEMs and DEPs in the cholesterol metabolism, NF-kappaB and phospholipase D signaling pathways. (A) Enrichment of DEMs and DEPs in the cholesterol metabolism signaling pathway. (B) Enrichment of DEMs and DEPs in the NF-kappaB signaling pathway. (C) Enrichment of DEMs and DEPs in the phospholipase D signaling pathway. (D) The correlation network of the DEMs and DEPs in the cholesterol metabolism signaling pathway. Blue circles represent metabolites, red circles represent proteins, red lines represent positive correlations, and blue lines represent negative correlations. (E) The correlation network of the DEMs and DEPs in the bile secretion signaling pathway. Blue circles represent metabolites, red circles represent proteins, red lines represent positive correlations, and blue lines represent negative correlations. (F) The cholesterol metabolism pathway; the upregulated metabolites are indicated in red. DEMs, differentially expressed metabolites; DEPs, differentially expressed proteins; SD-PD, stable disease-progressive disease; CR-PR, complete response-partial response; APOH, apolipoprotein H.

pathway (Fig. 2C). This suggests that the poor prognosis of patients in the SD/PD group may be related to these three pathways.

Moreover, widely targeted metabolomics showed that a total of 74 metabolites were downregulated and 60 metabolites were upregulated (Fig. 3A). The top ten up or downregulated metabolites are shown in Fig. 3B. KEGG enrichment analysis of the differentially expressed metabolites showed that these were mainly enriched in the 'NF-kappaB signaling pathway', the 'primary bile acid biosynthesis', the 'cholesterol metabolism' (Fig. 3C), suggesting that the poor prognosis of patients in the SD/PD group may be related to these pathways.

Proteomic changes of the SD/PD and CR/PR groups after immunotherapy. Quantitative proteomic analysis was performed on the plasma samples of both groups to elucidate the proteomic changes in the SD/PD group. MS data were acquired using the DIA mode, which combined the advantages of traditional shotgun proteomics with those of the selected/multiple reaction monitoring (SRM/MRM) technique, a technique considered as the 'gold standard' for MS-based absolute quantification. The entire scan range of the mass spectrometer was divided into several windows by m/z, and all parent ions in each window were then fragmented and detected, followed by collecting and using the fragmentation information of all parent ions for protein characterization and quantification. First of all, data were searched against the Swiss-Prot Human database and the results were filtered at 1% FDR, which identified 12,365 peptides and 1,535 proteins. Second, 113 differentially expressed proteins were identified, comprising 50 upregulated proteins and 63 downregulated proteins (Fig. 4A). For better observation of protein change patterns, proteins with significant differential expression were normalized and a clustered heat map was generated. This showed that protein expression profiles were significantly different between the CR/PR and SD/PD groups (Fig. 4B). Next, all differentially expressed proteins were subjected to enrichment analysis for GO categories using ClusterProfiler (33) and the results are shown in Fig. 4C. KEGG pathway enrichment analysis revealed that differentially expressed proteins were mainly enriched in the 'PI3K-Akt signaling pathway', the 'NF-kappaB signaling pathway', and the 'phospholipase D signaling pathway' (Fig. 4D).

Combined metabolomic and proteomic analysis. Correlation analysis between proteomic and metabolomic data was performed to elucidate the mutual regulatory relationship between differentially expressed proteins and metabolites. First of all, the common KEGG pathways wherein both differentially expressed proteins and metabolites were enriched were identified according to KEGG pathway enrichment analysis. The combined analysis of widely targeted proteomic and lipidomic data showed that DEMs and DEPs were enriched in the 'cholesterol metabolism' pathway (Fig. 5A). The combined analysis of widely targeted metabolomic and proteomic data showed that DEPs and DEMs were enriched in the 'NF-kappaB signaling pathway' and in the 'phospholipase D signaling pathway' (Fig. 5B). The results indicated that the PD-1 monoclonal antibody resistance may be attributed to the three metabolic signalling pathways.

Cholesterol metabolism, NF-kappaB, and phospholipase D signalling pathway analysis. Considering that cholesterol metabolism, NF-kappaB, and phospholipase D signalling pathways play important roles in PD-1 monoclonal antibody resistance in patients with OSCC, the enrichment of DEMs and DEPs was then analysed in these pathways in detail. The heatmap showed that the expression of triglyceride, cholesteryl ester, and apolipoprotein H (APOH) was upregulated in the SD/PD group (Fig. 6A), indicating that the cholesterol metabolism signalling pathway was correlated with the poor prognosis of patients with OSCC treated with immunotherapy combined with chemotherapy. The expression of IGHV6-1, IGHV3-72, IGHV1-18, IGHV3-11, IGHV2-70, IGHV1-2, LY96, IGHV2-5, KIT and d-myo-inositol-1,4,5-triphosphate enrichment in the NF-kappaB and phospholipase D signalling pathway was also upregulated (Fig. 6B and C), suggesting that the NF-kappaB and phospholipase D signalling pathway was activated to promote the immunotherapy and chemotherapy resistance of OSCC. The process described above indicates that the proteins target metabolites to regulate a series of pathways. Clarifying the correlation between the proteins and metabolites is essential for further screening of the mechanisms of resistance to the PD-1 monoclonal antibody in patients with OSCC. The results showed that TG, CE, glycochenodeoxycholic acid, glycocholic acid, and taurocholic acid were co-regulated by APOH (Fig. 6D and E), indicating that APOH may contribute to the immunotherapy and chemotherapy resistance by regulating the metabolism of TG, CE, glycochenodeoxycholic acid, glycocholic acid, and taurocholic acid. Cholesterol metabolism is described in Fig. 6F.

Discussion

In recent years, an increasing number of studies have used MS to identify biomarkers of oesophageal cancer. In one study, non-targeted metabolomics was performed on tumour tissues from 15 patients with stage I, II, III, and IV OSCC and 15 control individuals with normal oesophageal tissues, and the results showed that glycerophosphate metabolism played an important role in the development and progression of OSCC (34). A database search showed that glycerophospholipid metabolism genes, phosphatidylserine synthase 1 (PTDSS1) and lysophosphatidylcholine acyltransferase 1 (LPCAT1), can predict prognosis in patients with OSCC (34). A targeted LC-MS/MS assay performed on serum samples from 320 patients with oesophageal cancer and 323 healthy individuals revealed that d-mannose was significantly upregulated in the serum of patients with oesophageal cancer and could be used as a potential biomarker for the diagnosis of oesophageal cancer (35). Liquid chromatography-quadrupole/time-of-flight mass spectrometry (LC-Q/TOF-MS)-based non-targeted metabolomic examination of the serum samples of 40 patients with OSCC and 10 healthy individuals revealed that phosphatidylcholine metabolism was significantly abnormal in the serum of patients with OSCC (36). LC-MS and NMR analysis revealed that metabolites abnormally expressed in patients with oesophageal adenocarcinoma included β-hydroxybytyrate, lysine, glutamine, citrate, creatinine, lactate, and glucose (37). Furthermore, serum proline was found to be expressed at

reduced levels in patients with oesophageal cancer and can be used as a risk marker for early diagnosis of patients with oesophageal cancer (38). A total of seven glycoproteins and 13 glycopeptides were found to be upregulated in patients with oesophageal cancer (39). An LC-MS-based study identified 20 OSCC-related biomarkers, of which nine metabolites were associated with *in situ* tumour metastasis, lymph node metastasis, and OS. Glutamate was associated with *in situ* tumour metastasis; oleic acid, LysoPC (15:0), uracil, inosine, and choline were associated with lymph node metastasis; and glutamine, kynurenine, serine, and uracil were associated with OS (40).

Numerous studies have been conducted in recent years to explore the proteomic changes of patients with oesophageal cancer (41-44). By using Isobaric Tags for Relative and Absolute Quantification (iTRAQ), one study identified 516 differentially expressed proteins in oesophageal cancer tissues and normal tissues adjacent to the cancer, in which N-alpha-acetyltransferase 10 (NAA10) was expressed at reduced levels in oesophageal cancer tissues and NAA10 inhibited the proliferation of OSCC cells; this suggests that NAA10 may serve as a suppressor of OSCC and a new potential diagnostic biomarker for OSCC (45). In addition, the regulatory mechanism of MARCH8 has been elucidated using the iTRAQ technique (46). A combined application of iTRAQ and 2D-LC-MS/MS identified 90 differentially expressed proteins in 28 patients with OSCC and healthy individuals, including extracellular matrix protein 1 (ECM1) and lumican (LUM), which were subsequently shown to promote the proliferation and metastasis of OSCC cells (47). Using iTRAQ proteomics, one study identified 431 proteins differentially expressed in OSCC tissues relative to paracancerous tissues, such as 4-hydroxylase subunit α-1, prolyl4-hydroxylase subunit α-2, calponin-2, immunoglobulin superfamily containing leucine-rich repeat protein, and 3-hydroxylase 1 (48). Liu *et al* used large-scale and high-resolution MS-based proteomics to classify oesophageal cancer into two subtypes, SI and S2, with the S2 subtype characterized by upregulation of spliceosomal and ribosomal proteins as the biomarker (49). A total of 9,042 proteins and 26,892 phosphosites were identified through extensive proteomic and phosphoproteomic analysis based on iTRAQ, including 556 differentially expressed proteins and 1,691 differentially expressed phosphorylation sites; protein levels of the spliceosome pathway and phosphorylated protein levels were significantly upregulated in patients with stage III oesophageal cancer with the poorest postoperative prognosis, and CDC-like kinase may serve as a potential therapeutic target for patients with OSCC (50).

The NF-κB pathway plays an important role in the development and progression of tumours. Activation of this pathway can upregulate downstream pro- and anti-apoptotic gene expression and can regulate a range of signalling pathways to promote tumour cell proliferation and inhibit apoptosis, including the signalling pathways of STAT3, API, interferon, regulatory factors, NRF2, Notch, WNT-β-catenin, and p53 (51-54). In addition, the NF-κB pathway and inflammation can promote genomic, epigenetic, and metabolomic alterations that lead to the epithelial-to-mesenchymal transition (EMT), metastasis, and invasion of tumour cells, resulting in tumour resistance to immune drugs (55-57). Bulk and single-cell transcriptomic analyses revealed that clinical patients treated effectively with anti-CTLA4 and anti-PD1 showed upregulation of NF-κB pathway genes in both tumour cells and immune cells (58). Moreover, a large number of NF-κB-regulated cytokines and chemokines were up- or downregulated in patients who responded well to immunotherapy (59). CD28 binding leads to activation of the NF-κB pathway through a number of processes, which plays an important role in the *in vivo* anti-PD-1 treatment of mice (59). In addition, two classical NF-κB pathway-dependent genes, IFNγ and CD127, can enhance the efficacy of dual CTLA-4/PD-1 inhibition (60). It has been widely demonstrated that activation of the NF-κB pathway significantly enhances the efficacy of tumour immunotherapy (61-63). Numerous studies have shown that inhibitors of the NF-κB pathway can inhibit tumour cell survival, proliferation, and invasion both *in vivo* and *in vitro*, possibly by promoting the maturation of DC cells and enhancing the antitumor activity of T and NK cells (64-66).

The phospholipase D family is widely distributed in cells. Phospholipase D isoforms (PLDs) and their hydrolysis product phosphatidic acid (PA) have been shown to be involved in the proliferation and metastasis of a variety of cancers. Both PLDs and PA can promote the activation of mTOR and can promote the expression of growth factor receptors, forming positive feedback with the wingless-related integration site protein (Wnt)/β-catenin/transcription factor 4 (TCF-4) pathway, thereby promoting tumour cell survival. They can also act as second messengers for numerous growth factors to promote cascade signal amplification. PLDs and PAs can promote tumour cell survival under nutrient deficiency. In the case of insufficient glucose levels, PLD-1 can provide energy to tumour cells by activating autophagy (67). In addition, PLDs and PAs are involved in mitochondria-mediated apoptotic processes. Mitochondrial cardiolipin deficiency leads to the downregulation of cytochrome, which causes activation of caspase-9 and caspase-3 and in turn activation of caspase cascade reaction, thereby promoting apoptosis (68). PA is an important intermediate metabolite for cardiolipin synthesis. Conversely, PLDs and PA can promote tumour invasion and metastasis. In particular, PLD2 plays an important role in SNAI1 and SNAI2-mediated EMT (69). PLDs and PA can promote the binding of NF-κB with specificity protein 1, which in turn promotes the expression of SP1, thereby increasing the degradation of the extracellular matrix (70). By regulating the PI3K/Akt and mitogen-activated protein kinase/ERK pathways, PLDs and PA can activate HIFs to promote the production of pro-angiogenic downstream targets and the phosphorylation of sphingosine kinase to sphingosine-1-phosphate, thereby activating VEGF receptors to promote tumour angiogenesis. The metastasis of vascular endothelial cells was promoted by upregulating the expression of MMPs and releasing Cripto-1. Some inhibitors of PLDs, such as resveratrol, quercetin, and honokiol have also been shown to have antitumor effects (71-73).

Cholesterol is a precursor of bile acids and cholesterol hormones, and has been shown to promote the development and progression of colon, breast, and prostate cancers. It also regulates tumour development and progression by modulating a range of signalling pathways involved therein. Tumour cells require large amounts of cholesterol to meet

the metabolic requirements of their rapid proliferation, such as the requirements for cell formation and other physiological functions (74). For example, 6-oxo-cholestan-3β,5α-diol has been revealed to be highly expressed in patients with breast cancer (75), and to promote tumour progression by binding to the glucocorticoid receptor. Therefore, cholesterol metabolism can promote tumour progression, including tumour cell proliferation, metastasis, and invasion (76-79). During cholesterol metabolism, immunosuppressive cells such as neutrophils (80), myeloid-derived suppressor cells (81), and tumour-associated macrophages (82) may be recruited to the tumour microenvironment, where they promote tumour progression, or suppress tumour regression by enhancing the function of T cells (83). In short, due to the important role of cholesterol metabolism in tumour progression, its inhibitors such as strains (84), lipophilic statins (85), R408-8071 (86), and zaragonic acids (87) are mostly used in the clinical treatment of tumours.

The NF-κB pathway, phospholipase D family and cholesterol metabolism pathway play an important role in the tumour progression. In the present study, the three aforementioned signalling pathways were identified using metabolomics and proteomics as being involved in the molecular mechanisms of anti-PD-1 monoclonal antibody resistance in patients with OSCC. More importantly, it was hypothesized that the resistance of anti-PD-1 monoclonal antibodies induced by cholesterol may be regulated by APOH. APOH also promotes progression in various cancers. For example, it was negatively related to prognosis in colorectal cancer (88) and hepatocellular carcinoma (89). In addition, APOH may be a promising non-invasive biomarker for renal cancer (90). A previous study found that as an immune-related gene, APOH could predict prognosis in early stage lung squamous cell carcinoma (91) and gastric cancer (92). However, the present study was limited by the small sample size and the lack of validation samples. Therefore, plasma samples from patients with OSCC undergoing treatment with anti-PD-1 monoclonal antibodies will be collected in the future to perform targeted metabolomics and proteomics to clarify the metabolites, metabolic pathways, and molecular mechanisms involved in anti-PD-1 monoclonal antibody resistance in patients with OSCC. Animal models of OSCC where the mice are treated with PD-1 monoclonal antibody alone, chemotherapy alone, and their combination will also be examined using metabolic/proteomic analysis to elucidate the DEPs and the DEMs between the chemoresistance alone group and the combination resistance group, and between the PD-1 monoclonal antibody resistance group and the combination resistance group, and thus investigate the potential interactions between the two therapies which lead to the immunotherapy resistance. Animal models and cell lines of OSCC will also be used to elucidate the molecular mechanisms of immunotherapy resistance in OSCC, and in addition, a search for low-molecular-weight drugs affecting metabolic pathways will be performed in order to enhance the sensitivity of immunotherapy in OSCC, and improve the prognosis of OSCC patients.

Acknowledgements

Not applicable.

Funding

The present study was funded by the Central Leading Local Science and Technology Development Special Foundation (grant no. ZYYD2020000169).

Availability of data and materials

The mass spectrometry proteomics data have been deposited to the ProteomeXchange Consortium (http://proteomecentral.proteomexchange.org) via the iProX partner repository with the dataset identifier PXD039045. URL: https://www.iprox.cn/page/PSV023.html;?url=16729105460717iE2. Password: I8Kh The raw metabolic data have already been submitted to the Metabolights database with an associated accession number of MTBLS6796 with the URL, www.ebi.ac.uk/metabolights/MTBLS6796.

Authors' contributions

LG substantially contributed to the conception of the study as well as the acquisition and analysis of the data. LG drafted the manuscript and YC revised it critically for important intellectual content. The funding was provided by YC. LG and YC confirm the authenticity of all the raw data. Both authors (LG and YC) read and approved the manuscript and agree to be accountable for all aspects of the research in ensuring that the accuracy or integrity of any part of the work are appropriately investigated and resolved.

Ethics approval and consent to participate

All procedures performed in studies involving human participants were conducted in accordance with the ethical standards of the institutional and national research committee and with the 1964 Declaration of Helsinki and its later amendments or comparable ethical standards. The study was approved (approval no. WDRY2020-K212) by the Bioethics Committee of Renmin Hospital of Wuhan University (Wuhan, Hubei). Written nformed consent was obtained from all participants included in the study.

Patient consent for publication

Not applicable.

Competing interests

The authors declare that they have no competing interests.

References

1. Bagchi S, Yuan R and Engleman EG: Immune checkpoint inhibitors for the treatment of cancer: Clinical impact and mechanisms of response and resistance. Annu Rev Pathol 16: 223-249, 2021.
2. Carlino MS, Larkin J and Long GV: Immune checkpoint inhibitors in melanoma. Lancet 398: 1002-1014, 2021.
3. Li F, Chen Y, Pang M, Yang P and Jing H: Immune checkpoint inhibitors and cellular treatment for lymphoma immunotherapy. Clin Exp Immunol 205: 1-11, 2021.
4. Kojima T, Shah MA, Muro K, Francois E, Adenis A, Hsu CH, Doi T, Moriwaki T, Kim SB, Lee SH, *et al*: Randomized phase III KEYNOTE-181 study of pembrolizumab versus chemotherapy in advanced esophageal cancer. J Clin Oncol 38: 4138-4148, 2020.

5. Kato K, Cho BC, Takahashi M, Okada M, Lin CY, Chin K, Kadowaki S, Ahn MJ, Hamamoto Y, Doki Y, *et al*: Nivolumab versus chemotherapy in patients with advanced oesophageal squamous cell carcinoma refractory or intolerant to previous chemotherapy (ATTRACTION-3): A multicentre, randomised, open-label, phase 3 trial. Lancet Oncol 20: 1506-1517, 2019.
6. Huang J, Xu J, Chen Y, Zhuang W, Zhang Y, Chen Z, Chen J, Zhang H, Niu Z, Fan Q, *et al*: Camrelizumab versus investigator's choice of chemotherapy as second-line therapy for advanced or metastatic oesophageal squamous cell carcinoma (ESCORT): A multicentre, randomised, open-label, phase 3 study. Lancet Oncol 21: 832-842, 2020.
7. Sun JM, Shen L, Shah MA, Enzinger P, Adenis A, Doi T, Kojima T, Metges JP, Li Z, Kim SB, *et al*: Pembrolizumab plus chemotherapy versus chemotherapy alone for first-line treatment of advanced oesophageal cancer (KEYNOTE-590): A randomised, placebo-controlled, phase 3 study. Lancet 398: 759-771, 2021.
8. Luo H, Lu J, Bai Y, Mao T, Wang J, Fan Q, Zhang Y, Zhao K, Chen Z, Gao S, *et al*: Effect of camrelizumab vs placebo added to chemotherapy on survival and progression-free survival in patients with advanced or metastatic esophageal squamous cell carcinoma: The ESCORT-1st randomized clinical trial. JAMA 326: 916-925, 2021.
9. Rinschen MM, Ivanisevic J, Giera M and Siuzdak G: Identification of bioactive metabolites using activity metabolomics. Nat Rev Mol Cell Biol 20: 353-367, 2019.
10. Muthubharathi BC, Gowripriya T and Balamurugan K: Metabolomics: Small molecules that matter more. Mol Omics 17: 210-229, 2021.
11. Chen PH, Cai L, Huffman K, Yang C, Kim J, Faubert B, Boroughs L, Ko B, Sudderth J, McMillan EA, *et al*: Metabolic diversity in human non-small cell lung cancer cells. Mol Cell 76: 838-851.e5, 2019.
12. Shen Y, Sun M, Zhu J, Wei M, Li H, Zhao P, Wang J, Li R, Tian L, Tao Y, *et al*: Tissue metabolic profiling reveals major metabolic alteration in colorectal cancer. Mol Omics 17: 464-471, 2021.
13. Li L and Ma J: Molecular characterization of metabolic subtypes of gastric cancer based on metabolism-related lncRNA. Sci Rep 11: 21491, 2021.
14. Chen CJ, Lee DY, Yu J, Lin YN and Lin TM: Recent advances in LC-MS-based metabolomics for clinical biomarker discovery. Mass Spectrom Rev: e21785, 2022 (Epub ahead of print).
15. Seger C and Salzmann L: After another decade: LC-MS/MS became routine in clinical diagnostics. Clin Biochem 82: 2-11, 2020.
16. Beccaria M and Cabooter D: Current developments in LC-MS for pharmaceutical analysis. Analyst 145: 1129-1157, 2020.
17. Zhang S, Wang H and Zhu MJ: A sensitive GC/MS detection method for analyzing microbial metabolites short chain fatty acids in fecal and serum samples. Talanta 196: 249-254, 2019.
18. Beale DJ, Pinu FR, Kouremenos KA, Poojary MM, Narayana VK, Boughton BA, Kanojia K, Dayalan S, Jones OAH and Dias DA: Review of recent developments in GC-MS approaches to metabolomics-based research. Metabolomics 14: 152, 2018.
19. Hu R, Li T, Yang Y, Tian Y and Zhang L: NMR-based metabolomics in cancer research. Adv Exp Med Biol 1280: 201-218, 2021.
20. Bichmann L, Gupta S, Rosenberger G, Kuchenbecker L, Sachsenberg T, Ewels P Alka O, Pfeuffer J, Kohlbacher O and Röst H: DIAproteomics: A multifunctional data analysis pipeline for data-independent acquisition proteomics and peptidomics. J Proteome Res 20: 3758-3766, 2021.
21. Ma L, Muscat JE, Sinha R, Sun D and Xiu G: Proteomics of exhaled breath condensate in lung cancer and controls using data-independent acquisition (DIA): A pilot study. J Breath Res 15: 026002, 2021.
22. Krasny L and Huang PH: Data-independent acquisition mass spectrometry (DIA-MS) for proteomic applications in oncology. Mol Omics 17: 29-42, 2021.
23. Zheng X, Xu K, Zhou B, Chen T, Huang Y, Li Q, Wen F, Ge W, Wang J, Yu S, *et al*: A circulating extracellular vesicles-based novel screening tool for colorectal cancer revealed by shotgun and data-independent acquisition mass spectrometry. J Extracell Vesicles 9: 1750202, 2020.
24. Rao J, Wan X, Tou F, He Q, Xiong A, Chen X, Cui W and Zheng Z: Molecular characterization of advanced colorectal cancer using serum proteomics and metabolomics. Front Mol Biosci 8: 687229, 2021.
25. Zhang Q, Zhang Y, Sun S, Wang K, Qian J, Cui Z, Tao T and Zhou J: ACOX2 is a prognostic marker and impedes the progression of hepatocellular carcinoma via PPARα pathway. Cell Death Dis 12: 15, 2021.
26. Kong R, Qian X and Ying W: Pancreatic cancer cells spectral library by DIA-MS and the phenotype analysis of gemcitabine sensitivity. Sci Data 9: 283, 2022.
27. Keam SP, Gulati T, Gamell C, Caramia F, Huang C, Schittenhelm RB, Kleifeld O, Neeson PJ, Haupt Y and Williams SG: Exploring the oncoproteomic response of human prostate cancer to therapeutic radiation using data-independent acquisition (DIA) mass spectrometry. Prostate 78: 563-575, 2018.
28. Sun Y, Li L, Zhou Y, Ge W, Wang H, Wu R, Liu W, Chen H, Xiao Q, Cai X, *et al*: Stratification of follicular thyroid tumours using data-independent acquisition proteomics and a comprehensive thyroid tissue spectral library. Mol Oncol 16: 1611-1624, 2022.
29. Oken MM, Creech RH, Tormey DC, Horton J, Davis TE, McFadden ET and Carbone PP: Toxicity and response criteria of the Eastern cooperative oncology group. Am J Clin Oncol 5: 649-655, 1982.
30. Schwartz LH, Litière S, de Vries E, Ford R, Gwyther S, Mandrekar S, Shankar L, Bogaerts J, Chen A, Dancey J, *et al*: RECIST 1.1-update and clarification: From the RECIST committee. Eur J Cancer 62: 132-137, 2016.
31. Greene FL, Page DL, Fleming ID, Fritz AG, Balch CM, Haller DG Morrow M (eds): AJCC cancer staging manual. 6th edition. American Joint Committe on Cancer, Chicago, IL, pp91-99, 2002.
32. Demichev V, Messner CB, Vernardis SI, Lilley KS and Ralser M: DIA-NN: Neural networks and interference correction enable deep proteome coverage in high throughput. Nat Methods 17: 41-44, 2020.
33. Yu G, Wang LG, Han Y and He QY: clusterProfiler: An R package for comparing biological themes among gene clusters. OMICS 16: 284-287, 2012.
34. Yang T, Hui R, Nouws J, Sauler M, Zeng T and Wu Q: Untargeted metabolomics analysis of esophageal squamous cell cancer progression. J Transl Med 20: 127, 2022.
35. White L, Ma J, Liang S, Sanchez-Espiridion B and Liang D: LC-MS/MS determination of d-mannose in human serum as a potential cancer biomarker. J Pharm Biomed Anal 137: 54-59, 2017.
36. Mir SA, Rajagopalan P, Jain AP, Khan AA, Datta KK, Mohan SV, Lateef SS, Sahasrabuddhe N, Somani BL, Keshava Prasad TS, *et al*: LC-MS-based serum metabolomic analysis reveals dysregulation of phosphatidylcholines in esophageal squamous cell carcinoma. J Proteomics 127: 96-102, 2015.
37. Zhang J, Bowers J, Liu L, Wei S, Gowda GA, Hammoud Z and Raftery D: Esophageal cancer metabolite biomarkers detected by LC-MS and NMR methods. PLoS One 7: e30181, 2012.
38. Liang S, Sanchez-Espiridion B, Xie H, Ma J, Wu X and Liang D: Determination of proline in human serum by a robust LC-MS/MS method: Application to identification of human metabolites as candidate biomarkers for esophageal cancer early detection and risk stratification. Biomed Chromatogr 29: 570-577, 2015.
39. Song E, Zhu R, Hammoud ZT and Mechref Y: LC-MS/MS quantitation of esophagus disease blood serum glycoproteins by enrichment with hydrazide chemistry and lectin affinity chromatography. J Proteome Res 13: 4808-4820, 2014.
40. Zhang H, Wang L, Hou Z, Ma H, Mamtimin B, Hasim A and Sheyhidin I: Metabolomic profiling reveals potential biomarkers in esophageal cancer progression using liquid chromatography-mass spectrometry platform. Biochem Biophys Res Commun 491: 119-125, 2017.
41. Guo JH, Xing GL, Fang XH, Wu HF, Zhang B, Yu JZ, Fan ZM and Wang LD: Proteomic profiling of fetal esophageal epithelium, esophageal cancer, and tumor-adjacent esophageal epithelium and immunohistochemical characterization of a representative differential protein, PRX6. World J Gastroenterol 23: 1434-1442, 2017.
42. Yazdian-Robati R, Ahmadi H, Riahi MM, Lari P, Aledavood SA, Rashedinia M, Abnous K and Ramezani M: Comparative proteome analysis of human esophageal cancer and adjacent normal tissues. Iran J Basic Med Sci 20: 265-271, 2017.
43. O'Neill JR, Pak HS, Pairo-Castineira E, Save V, Paterson-Brown S, Nenutil R, Vojtěšek B, Overton I, Scherl A and Hupp TR: Quantitative shotgun proteomics unveils candidate novel esophageal adenocarcinoma (EAC)-specific proteins. Mol Cell Proteomics 16: 1138-1150, 2017.

44. Schwacke J, Millar TP, Hammond CE, Saha A, Hoffman BJ, Romagnuolo J, Hill EG and Smolka AJ: Discrimination of normal and esophageal cancer plasma proteomes by MALDI-TOF mass spectrometry. Dig Dis Sci 60: 1645-1654, 2015.
45. Wang D, Chen J, Han J, Wang K, Fang W, Jin J and Xue S: iTRAQ and two-dimensional-LC-MS/MS reveal NAA10 is a potential biomarker in esophageal squamous cell carcinoma. Proteomics Clin Appl 16: e2100081, 2022.
46. Singh S, Bano A, Saraya A, Das P and Sharma R: iTRAQ-based analysis for the identification of MARCH8 targets in human esophageal squamous cell carcinoma. J Proteomics 236: 104125, 2021.
47. Wang X, Peng Y, Xie M, Gao Z, Yin L, Pu Y and Liu R: Identification of extracellular matrix protein 1 as a potential plasma biomarker of ESCC by proteomic analysis using iTRAQ and 2D-LC-MS/MS. Proteomics Clin Appl 11: 1600163, 2017.
48. Deng F, Zhou K, Li Q, Liu D, Li M, Wang H, Zhang W and Ma Y: iTRAQ-based quantitative proteomic analysis of esophageal squamous cell carcinoma. Tumour Biol 37: 1909-1918, 2016.
49. Liu W, Xie L, He YH, Wu ZY, Liu LX, Bai XF, Deng DX, Xu XE, Liao LD, Lin W, *et al*: Large-scale and high-resolution mass spectrometry-based proteomics profiling defines molecular subtypes of esophageal cancer for therapeutic targeting. Nat Commun 12: 4961, 2021.
50. Li Y, Yang B, Ma Y, Peng X, Wang Z, Sheng B, Wei Z, Cui Y and Liu Z: Phosphoproteomics reveals therapeutic targets of esophageal squamous cell carcinoma. Signal Transduct Target Ther 6: 381, 2021.
51. Joyce D, Albanese C, Steer J, Fu M, Bouzahzah B and Pestell RG: NF-kappaB and cell-cycle regulation: the cyclin connection. Cytokine Growth Factor Rev 12: 73-90, 2001.
52. Grivennikov SI and Karin M: Dangerous liaisons: STAT3 and NF-kappaB collaboration and crosstalk in cancer. Cytokine Growth Factor Rev 21: 11-19, 2010.
53. Vanden Berghe T, Linkermann A, Jouan-Lanhouet S, Walczak H and Vandenabeele P: Regulated necrosis: The expanding network of non-apoptotic cell death pathways. Nat Rev Mol Cell Biol 15: 135-147, 2014.
54. Taniguchi K, Wu LW, Grivennikov SI, de Jong PR, Lian I, Yu FX, Wang K, Ho SB, Boland BS, Chang JT, *et al*: A gp130-Src-YAP module links inflammation to epithelial regeneration. Nature 519: 57-62, 2015.
55. Johnson RF and Perkins ND: Nuclear factor-κB, p53, and mitochondria: Regulation of cellular metabolism and the Warburg effect. Trends Biochem Sci 37: 317-324, 2012.
56. Xia Y, Shen S and Verma IM: NF-κB, an active player in human cancers. Cancer Immunol Res 2: 823-830, 2014.
57. Wu Y and Zhou BP: Inflammation: A driving force speeds cancer metastasis. Cell Cycle 8: 3267-3273, 2009.
58. Amato CM, Hintzsche JD, Wells K, Applegate A, Gorden NT, Vorwald VM, Tobin RP, Nassar K, Shellman YG, Kim J, *et al*: Pre-treatment mutational and transcriptomic landscape of responding metastatic melanoma patients to anti-PD1 immunotherapy. Cancers (Basel) 12: 1943, 2020.
59. Roh W, Chen PL, Reuben A, Spencer CN, Prieto PA, Miller JP, Gopalakrishnan V, Wang F, Cooper ZA, Reddy SM, *et al*: Integrated molecular analysis of tumor biopsies on sequential CTLA-4 and PD-1 blockade reveals markers of response and resistance. Sci Transl Med 9: eaah3560, 2017.
60. Shi LZ, Fu T, Guan B, Chen J, Blando JM, Allison JP, Xiong L, Subudhi SK, Gao J and Sharma P: Interdependent IL-7 and IFN-γ signalling in T-cell controls tumour eradication by combined α-CTLA-4+α-PD-1 therapy. Nat Commun 7: 12335, 2016.
61. Dong MB, Wang G, Chow RD, Ye L, Zhu L, Dai X, Park JJ, Kim HR, Errami Y, Guzman CD, *et al*: Systematic immunotherapy target discovery using genome-scale in vivo CRISPR screens in CD8 T cells. Cell 178: 1189-1204.e23, 2019.
62. Li G, Boucher JC, Kotani H, Park K, Zhang Y, Shrestha B, Wang X, Guan L, Beatty N, Abate-Daga D and Davila ML: 4-1BB enhancement of CAR T function requires NF-κB and TRAFs. JCI Insight 3: e121322, 2018.
63. Philipson BI, O'Connor RS, May MJ, June CH, Albelda SM and Milone MC: 4-1BB costimulation promotes CAR T cell survival through noncanonical NF-κB signaling. Sci Signal 13: eaay8248, 2020.
64. Schumacher LY, Vo DD, Garban HJ, Comin-Anduix B, Owens SK, Dissette VB, Glaspy JA, McBride WH, Bonavida B, Economou JS and Ribas A: Immunosensitization of tumor cells to dendritic cell-activated immune responses with the proteasome inhibitor bortezomib (PS-341, Velcade). J Immunol 176: 4757-4765, 2006.
65. Enzler T, Sano Y, Choo MK, Cottam HB, Karin M, Tsao H and Park JM: Cell-selective inhibition of NF-κB signaling improves therapeutic index in a melanoma chemotherapy model. Cancer Discov 1: 496-507, 2011.
66. Xiao Z, Su Z, Han S, Huang J, Lin L and Shuai X: Dual pH-sensitive nanodrug blocks PD-1 immune checkpoint and uses T cells to deliver NF-κB inhibitor for antitumor immunotherapy. Sci Adv 6: eaay7785, 2020.
67. Cai M, He J, Xiong J, Tay LW, Wang Z, Rog C, Wang J, Xie Y, Wang G, Banno Y, *et al*: Phospholipase D1-regulated autophagy supplies free fatty acids to counter nutrient stress in cancer cells. Cell Death Dis 7: e2448, 2016.
68. Palikaras K, Lionaki E and Tavernarakis N: Mechanisms of mitophagy in cellular homeostasis, physiology and pathology. Nat Cell Biol 20: 1013-1022, 2018.
69. Ganesan R, Mallets E and Gomez-Cambronero J: The transcription factors Slug (SNAI2) and Snail (SNAI1) regulate phospholipase D (PLD) promoter in opposite ways towards cancer cell invasion. Mol Oncol 10: 663-676, 2016.
70. Ho HY, Lin CW, Chien MH, Reiter RJ, Su SC, Hsieh YH and Yang SF: Melatonin suppresses TPA-induced metastasis by downregulating matrix metalloproteinase-9 expression through JNK/SP-1 signaling in nasopharyngeal carcinoma. J Pineal Res 61: 479-492, 2016.
71. Issuree PD, Pushparaj PN, Pervaiz S and Melendez AJ: Resveratrol attenuates C5a-induced inflammatory responses in vitro and in vivo by inhibiting phospholipase D and sphingosine kinase activities. FASEB J 23: 2412-2424, 2009.
72. Park MH and Min do S: Quercetin-induced downregulation of phospholipase D1 inhibits proliferation and invasion in U87 glioma cells. Biochem Biophys Res Commun 412: 710-715, 2011.
73. Garcia A, Zheng Y, Zhao C, Toschi A, Fan J, Shraibman N, Brown HA, Bar-Sagi D, Foster DA and Arbiser JL: Honokiol suppresses survival signals mediated by Ras-dependent phospholipase D activity in human cancer cells. Clin Cancer Res 14: 4267-4274, 2008.
74. Huang B, Song BL and Xu C: Cholesterol metabolism in cancer: Mechanisms and therapeutic opportunities. Nat Metab 2: 132-141, 2020.
75. Voisin M, de Medina P, Mallinger A, Dalenc F, Huc-Claustre E, Leignadier J, Serhan N, Soules R, Ségala G, Mougel A, *et al*: Identification of a tumor-promoter cholesterol metabolite in human breast cancers acting through the glucocorticoid receptor. Proc Natl Acad Sci USA 114: E9346-E9355, 2017.
76. Chimento A, Casaburi I, Avena P, Trotta F, De Luca A, Rago V, Pezzi V and Sirianni R: Cholesterol and its metabolites in tumor growth: Therapeutic potential of statins in cancer treatment. Front Endocrinol (Lausanne) 9: 807, 2019.
77. Ding X, Zhang W, Li S and Yang H: The role of cholesterol metabolism in cancer. Am J Cancer Res 9: 219-227, 2019.
78. Wang Y, Liu C and Hu L: Cholesterol regulates cell proliferation and apoptosis of colorectal cancer by modulating miR-33a-PIM3 pathway. Biochem Biophys Res Commun 511: 685-692, 2019.
79. Liu Z, Liu X, Liu S and Cao Q: Cholesterol promotes the migration and invasion of renal carcinoma cells by regulating the KLF5/miR-27a/FBXW7 pathway. Biochem Biophys Res Commun 502: 69-75, 2018.
80. Raccosta L, Fontana R, Maggioni D, Lanterna C, Villablanca EJ, Paniccia A, Musumeci A, Chiricozzi E, Trincavelli ML, Daniele S, *et al*: The oxysterol-CXCR2 axis plays a key role in the recruitment of tumor-promoting neutrophils. J Exp Med 210: 1711-1728, 2013.
81. Condamine T, Dominguez GA, Youn JI, Kossenkov AV, Mony S, Alicea-Torres K, Tcyganov E, Hashimoto A, Nefedova Y, Lin C, *et al*: Lectin-type oxidized LDL receptor-1 distinguishes population of human polymorphonuclear myeloid-derived suppressor cells in cancer patients. Sci Immunol 1: aaf8943, 2016.
82. Goossens P, Rodriguez-Vita J, Etzerodt A, Masse M, Rastoin O, Gouirand V, Ulas T, Papantonopoulou O, Van Eck M, Auphan-Anezin N, *et al*: Membrane cholesterol efflux drives tumor-associated macrophage reprogramming and tumor progression. Cell Metab 29: 1376-1389.e4, 2019.
83. Kidani Y, Elsaesser H, Hock MB, Vergnes L, Williams KJ, Argus JP, Marbois BN, Komisopoulou E, Wilson EB, Osborne TF, *et al*: Sterol regulatory element-binding proteins are essential for the metabolic programming of effector T cells and adaptive immunity. Nat Immunol 14: 489-499, 2013.

84. Larsen SB, Dehlendorff C, Skriver C, Dalton SO, Jespersen CG, Borre M, Brasso K, Nørgaard M, Johansen C, Sørensen HT, *et al*: Postdiagnosis statin use and mortality in danish patients with prostate cancer. J Clin Oncol 35: 3290-3297, 2017.
85. Xia Y, Xie Y, Yu Z, Xiao H, Jiang G, Zhou X, Yang Y, Li X, Zhao M, Li L, *et al*: The mevalonate pathway is a druggable target for vaccine adjuvant discovery. Cell 175: 1059-1073.e21, 2018.
86. Maione F, Oliaro-Bosso S, Meda C, Di Nicolantonio F, Bussolino F, Balliano G, Viola F and Giraudo E: The cholesterol biosynthesis enzyme oxidosqualene cyclase is a new target to impair tumour angiogenesis and metastasis dissemination. Sci Rep 5: 9054, 2015.
87. Lanterna C, Musumeci A, Raccosta L, Corna G, Moresco M, Maggioni D, Fontana R, Doglioni C, Bordignon C, Traversari C and Russo V: The administration of drugs inhibiting cholesterol/oxysterol synthesis is safe and increases the efficacy of immunotherapeutic regimens in tumor-bearing mice. Cancer Immunol Immunother 65: 1303-1315, 2016.
88. Lu Y, Wang Y, Qiu Y and Xuan W: Analysis of the relationship between the expression level of TTR and APOH and prognosis in patients with colorectal cancer metastasis based on bioinformatics. Contrast Media Mol Imaging 2022: 1121312, 2022.
89. Li X, Wang L, Wang L, Feng Z and Peng C: Single-cell sequencing of hepatocellular carcinoma reveals cell interactions and cell heterogeneity in the microenvironment. Int J Gen Med 14: 10141-10153, 2021.
90. Mandili G, Notarpietro A, Khadjavi A, Allasia M, Battaglia A, Lucatello B, Frea B, Turrini F, Novelli F, Giribaldi G and Destefanis P: Beta-2-glycoprotein-1 and alpha-1-antitrypsin as urinary markers of renal cancer in von Hippel-Lindau patients. Biomarkers 23: 123-130, 2018.
91. Fan T, Lu Z, Liu Y, Wang L, Tian H, Zheng Y, Zheng B, Xue L, Tan F, Xue Q, *et al*: A novel immune-related seventeen-gene signature for predicting early stage lung squamous cell carcinoma prognosis. Front Immunol 12: 665407, 2021.
92. Qiu XT, Song YC, Liu J, Wang ZM, Niu X and He J: Identification of an immune-related gene-based signature to predict prognosis of patients with gastric cancer. World J Gastrointest Oncol 12: 857-876, 2020.